Electronic supplementary information available

Geometrically isomeric [Ir(iqbt)(ppy)(hpa)] complexes with differential molecule orientations for efficient near-infrared (NIR) polymer light-emitting diodes (PLEDs)

Wentao Li,‡[a] Jiaxiang Liu,‡[a] Baowen Wang,[a] Siyu Hou,[a] Xingqiang Lü,[a,*] Guorui Fu[a,b*] and Wai-Yeung Wong[b,*]

Supporting information

Materials and methods

All reagents were received from Sigma Aldrich and used without further purification. All solvents unless otherwise stated were degassed and stored over 3 Å activated molecular sieves prior to use. All manipulations of air and water sensitive compounds were carried out under dry N_2 using the standard Schlenk line techniques.

Elemental analysis (EA) was performed on a Perkin-Elmer 240C elemental analyzer. Fourier Transform Infrared (FT-IR) spectra were recorded on a Nicolet Nagna-IR 550 spectrophotometer in the region 4000-400 cm^{-1} using KBr pellets. ^1H NMR spectra were recorded on a JEOL EX 400 spectrometer with $SiMe_4$ as internal standard in $CDCl_3$ or DMSO-d_6 at room temperature. Electro-spray ionization mass spectrometry (ESI-MS) was performed on a Finnigan LCQ^{DECA} XP HPLC-MS$_n$ mass spectrometer with a mass to charge (m/z) range of 4000 using a standard electro-spray ion source and CH_2Cl_2 as the solvent.

Electronic absorption spectra in the UV-visible-NIR region were recorded with a Cary 300 UV spectrophotometer. Visible or NIR emission and excitation spectra were collected by a combined fluorescence lifetime and steady-state spectrometer (FLS-980, Edinburgh) with a 450 W Xe lamp. Excited-state decay times were obtained by the same spectrometer but with a μF900 Xe lamp. The quantum yield (Φ_{PL}) in solution was measured with free-base tetraphenylporphyrin (Φ_r = 0.13 in toluene solution at 298 K) as the standard.[1] The solution was degassed by three freeze-pump-thaw circles. The following equation was used to calculate the quantum yields:

$$\Phi_s = \Phi_r \times [(n_s^2 \times A_r \times I_s)/(n_r^2 \times A_s \times I_r)]$$

where Φ_s is the quantum yield of the sample, Φ_r is the quantum yield of the reference, n_s is the refractive index of the sample, n_r is the refractive index of the reference, A_s and A_r are the absorbance of the sample and the reference at the wavelength of excitation (355 nm), respectively, and the I_s and I_r are the integrated areas of emission bands of the sample and the reference from 600 to 900 nm, which were recorded by a red photomultiplier tube (PMT) detector. Thermal properties were characterized using thermogravimetric (TG) analyses on a NETZSCH TG 209 instrument under a flow of nitrogen at a heating rate of 10 °C/min.

Synthesis of the C^N[1] ligand Hiqbt (1-(benzo[b]-thiophen-2-yl)-isoquinoline)

The C^N[1] ligand **Hiqbt** was synthesized from the improved Suzuki coupling reaction of 2-chloro-isoquinoline[2] (instead of 2-bromo-isoquinoline[3]) with benzo[b]thien-2-yl boronic acid. A mixture of 2-chloro-isoquinoline (0.653 g, 4.0 mmol) and benzo[b]thien-2-y boronic acid (0.713 g, 4.0 mmol) was dissolved into absolute mixed solvents of toluene-EtOH (60 mL; v/v

= 2:1) under a N$_2$ atmosphere. Then an aqueous solution (20 mL) of Na$_2$CO$_3$ (2 M) was added, and the mixture was degassed by a N$_2$ flow. Anhydrous Pd(PPh$_3$)$_4$ (190 mg, 0.2 mmol; 5 mol%) was added to the reaction mixture which was then heated at 85 °C for 48 h. The complete consumption of reagents was monitored by thin-layer chromatography (TLC) (Hexane/AcOEt, v/v = 9:1; R_f = 0.25). After cooling to room temperature, the organic phase was washed with brine and extracted with absolute CH$_2$Cl$_2$ (3×20 mL) three times. The combined organic phase was dried over anhydrous Na$_2$SO$_4$, and further purified with flash-column chromatography on silica gel (Hexane/AcOEt, v/v = 9:1), affording an off-white solid. Yield: 0.762 g (73%). Calcd for C$_{17}$H$_{11}$NS: C, 78.13; H, 4.24; N, 5.36%. Found: C, 78.05; H, 4.36; N, 5.29%. ^{1}H NMR (400 MHz, DMSO-d_6): δ (ppm) 8.70 (d, 1H, -Py), 8.61 (d, 1H, -Ph), 8.19 (s, 1H, -Th), 8.11 (d, 1H, -Ph), 8.06 (m, 1H, -Ph), 8.02 (m, 1H, -Py), 7.88 (m, 2H, -Ph), 7.81 (m, 1H, -Ph), 7.46 (m, 2H, -Ph).

Kamal M. Dawood [1],
*
Manahil B. Elamin, and Ahmad M. Farag

Synthesis and isolation of the [Ir(C^N^1)(C^N^2)(N^O)]-*tris*-heteroleptic isomeric products (1a and 1b)

To a stirred solution of the equimolar amount of the ligands of C^N^1-**Hiqbt** (288 mg, 1.10 mmol) and C^N^2-**Hppy** (170 mg, 1.10 mmol) in 2-ethoxyethanol/H$_2$O (30 mL; 3:1 (v/v)), IrCl$_3$·3H$_2$O (352 mg, 0.10 mmol) was added, the resultant mixture was heated to 110 °C and continuously stirred under a N$_2$ atmosphere for 24 h. After cooling to room temperature, the saturated brine (50 mL) was added, and the *in situ* formed μ-chloro-bridged dimer intermediates containing [Ir(iqbt)(ppy)(μ-Cl)]$_2$ were collected by filtration. Subsequently, after drying, the μ-chloro-bridged dimer intermediates, *t*-BuOK (3.0 equiv.) and **Hpa** (3.0

equiv.) were added to anhydrous CH_2Cl_2 (30 mL), and the reaction mixture was continuously stirred at room temperature under a N_2 atmosphere for another 24 h. After dryness under vacuum, the residue was extracted with CH_2Cl_2, and the combined red organic phase was dried over anhydrous $MgSO_4$. The solvent was removed under reduced pressure, and the residue was further purified on preparative TLC plates with CH_2Cl_2/MeOH (100:1; v/v) as the eluent, and then with CH_2Cl_2/acetone (100:1; v/v) as the following eluent, affording to the desirable product and the by-products, respectively.

For the first eluted [Ir(ppy)$_2$(hpa)] (yellow powder; R_f = 0.75): Yield: 48 mg (15%). Calcd for $C_{28}H_{20}IrN_3O_3$: C, 52.65; H, 3.16; N, 6.58. Found: C, 52.66; H, 3.19; N, 6.61%. ^1H NMR (CDCl$_3$, 400 MHz): δ (ppm) 13.35 (s, 1H, -OH), 8.44 (d, 1H, -Py), 8.36 (d, 1H, -Py), 8.31 (d, 1H, -Py), 8.00-7.88 (m, 4H, -Py), 7.60 (d, 1H, -Py), 7.51 (m, 3H, -Py), 7.40 (t, 3H, -Ph), 7.32 (d, 1H, -Py), 7.08 (t, 1H, -Ph), 7.01 (d, 1H, -Py), 6.30 (d, 1H, -Ph), 5.94 (d, 1H, -Ph). ESI-MS (in CH_2Cl_2) m/z: 639.11 (100%), [M-H]$^+$. This characterization result was identical with that in the literature.[4]

For the second eluted **[Ir(iqbt)$_2$(hpa)]** (brown-red microcrystalline; R_f = 0.65): Yield: 61 mg (15%). Calcd for $C_{40}H_{24}IrN_3O_3S_2$: C, 56.46; H, 2.84; N, 4.94%. Found: C, 56.41; H, 2.92; N, 4.92%. ^1H NMR (CDCl$_3$, 400 MHz): δ (ppm) 12.91 (s, 1H, -OH for hpa), 9.12 (d, 1H, -Py for iqbt), 9.03 (d, 1H, -Py for iqbt), 8.38 (d, 1H, -Py), 8.00 (d, 1H, -Py), 7.95 (d, 1H, -Ph), 7.87 (m, 6H, -Ph), 7.78 (d, 1H, -Ph), 7.51 (q, 2H, -Py), 7.39 (q, 1H, -Ph), 7.31 (s, 2H, -Ph), 7.23 (t, 1H, -Py), 7.14 (t, 1H, -Ph), 6.82 (q, 1H, -Ph), 6.69 (q, 1H, -Ph), 6.42 (d, 1H, -Ph), 6.08 (d, 1H, -Ph). ESI-MS (in CH_2Cl_2) m/z: 713.07 (100%), [M-hpa]$^+$. This characterization result was identical with that in the literature.[5]

For the third eluted isomer **1a** (reddish orange microcrystalline; R_f = 0.55): Yield: 54 mg, 15%. Calcd for $C_{34}H_{22}N_3O_3SIr$: C, 54.83; H, 2.98; N, 5.64%. Found: C, 54.79; H, 3.02; N, 5.69%. FT-IR (KBr cm^{-1}): 2961 (w), 2920 (w), 2851 (w), 1728 (w), 1634 (w), 1597 (w), 1464 (w), 1439 (m), 1418 (w), 1379 (w), 1308 (w), 1252 (m), 1219 (w), 1065 (m), 1022 (m), 918 (w), 889 (w), 858 (w), 822 (w), 802 (s), 725 (m), 689 (s), 629 (w), 567 (w), 449 (w). ^1H NMR (400 MH$_Z$,

CDCl$_3$): δ (ppm) 13.77 (s, 1H, -OH for hpa), 9.05 (d, 1H, -Py for iqbt), 8.89 (d, 1H, -Py for hpa), 7.97 (d, 1H, -Py), 7.89 (t, 1H, -Py), 7.84 (dd, 1H, -Py), 7.75 (m, 3H, -Ph), 7.64 (m, 1H, -Py), 7.43 (m, 1H, -Py), 7.30 (d, 1H, Py), 7.26 (m, 1H, -Py), 7.22 (m, 2H, -Ph), 7.15 (m, 2H, -Ph), 6.95 (t, 1H, -Ph), 6.80 (m, 2H, -Ph), 6.43 (m, 1H, -Ph), 6.04 (d, 1H, -Ph). ESI-MS (in CH$_2$Cl$_2$) m/z: 744.85 (100%), [M-H]$^+$.

For the final eluted isomer **1b** (reddish orange microcrystalline; R_f = 0.40): Yield: 36 mg, 10%. Calcd for C$_{34}$H$_{22}$N$_3$O$_3$SIr: C, 54.83; H, 2.98; N, 5.64%. Found: C, 54.79; H, 3.02; N, 5.69%. FT-IR (KBr cm^{-1}): 2963 (w), 2922 (w), 2851 (w), 1728 (w), 1634 (w), 1597 (w), 1545 (w), 1464 (w), 1439 (m), 1418 (w), 1379 (w), 1307 (w), 1258 (m), 1065 (m), 1014 (s), 918 (w), 889 (w), 858 (w), 800 (vs), 756 (w), 725 (w), 689 (m), 629 (w), 567 (w), 449 (w). ^{1}H NMR (400 MH$_z$, CDCl$_3$): δ(ppm) 13.61 (s, 1H, -OH for hpa), 8.60 (d, 1H, -Py for iqbt), 8.01 (d, 1H, -Py for hpa), 7.89 (t, 2H, -Py), 7.85 (d, 1H, -Py), 7.76 (m, 2H, -Ph), 7.68 (d, 1H, -Py), 7.62 (d, 1H, -Py), 7.39 (d, 1H, -Py), 7.36 (m, 1H, -Py), 7.23 (t, 1H, -Ph), 7.19 (m, 1H, -Ph), 7.10 (m, 2H, -Ph), 6.90 (q, 2H, -Ph), 6.74 (t, 1H, -Ph), 6.33 (d, 1H, -Ph), 6.20 (d, 1H, -Ph). ESI-MS (in CH$_2$Cl$_2$) m/z: 744.85 (100%), [M-H]$^+$.

X-Ray Crystallography

Single crystals for the geometrical isomers **1a**·CHCl$_3$ and **1b** of suitable dimensions were mounted onto thin glass fibers. All the intensity data were collected on a Bruker APLEX-II CCD diffractometer (Mo-Ka radiation and λ = 0.71073 Å) in Φ and w scan modes. Structures were solved by Direct methods followed by difference Fourier syntheses, and then refined by full-matrix least-squares techniques against F^2 using SHELXTL.[6] All other non-hydrogen atoms were refined with anisotropic thermal parameters. Absorption corrections were applied using SADABS.[7] All hydrogen atoms were placed in calculated positions and refined

isotropically using a riding model. Crystallographic data, relevant atomic distances and bond angles for the geometrical isomers **1a**·CHCl$_3$ and **1b** are presented in **Tables S1-2**, respectively. The CCDC numbers 2082463-2082464 for the geometrical isomers **1a**·CHCl$_3$ and **1b**, respectively.

Electronic structure calculations

To gain further insight into the photo-physical characteristics of the Ir(III)-complexes, theoretical studies on their electronic structures were carried out by using density functional theory (DFT) and time-dependent DFT (TD-DFT) methods. Each of their molecular structures was optimized at the ground state (S$_0$) and the first triplet state (T$_1$) in the gas phase. TD-DFT calculations using the B3LYP functional were then performed on the basis of the structural optimized geometries.[8] The 6-31G (d,p) basis set was applied for C, H, N, O, S atoms, while effective core potentials employed for Ir atom were based on a LanL2DZ basis set.[9-10] The energies of the excited states of the Ir(III)-complexes were computed by TD-DFT based on all the ground-state (S$_0$) and the first triplet state (T$_1$) geometries. Typically, the lowest triplet root of the nonhermitian eigenvalue equations was obtained to determine the vertical excitation energies. The first triplet state B3LYP and excited-state TDDFT calculations were carried out using Gaussian 09. Calculations of the dipole moment vectors (μ) of the different emitters were performed by DFT single point energy calculations using the hybrid functional B3LYP with the def2tzvp basis set based on the corresponding optimized S$_0$ and T$_1$ states. The contributions of fragments to the ''holes'' and ''electrons'' and Inter Fragment Charge Transfer (IFCT)[11] in the electronic excitation process were analyzed by the Ros and Schuit

method[12] (C-squared population analysis method, SCPA) in the Multiwfn 3.8 program.[13] All calculations were carried out with Gaussian 09, Revision D.01 software package.[14] The electron density diagrams of molecular orbitals were obtained with the ChemOffice 2010 graphics program.

Cyclic voltammetry (CV) measurement

Electro-chemical measurements were made using a Princeton Applied Research model 2273A potentiostat at a scan rate of 100 mV s^{-1}. A conventional three-electrode configuration consisting of a glassy carbon working electrode, a Pt-sheet counter electrode, and a Pt wire reference electrode was used. The supporting electrolyte was 0.1 M tetrabutylammonium tetrafluoroborate ([Bu$_4$N]BF$_4$) in MeCN. Ferrocene was added as a calibrant after each set of measurements, and all potentials reported are quoted with reference to the ferrocene–ferrocenium (Fc/Fc$^+$) couple. The HOMO and the LUMO energy levels of each complex are calculated according to the following equations,[15] $E_{HOMO} = -(E_{OX}^{1/2} - E_{ferrocene}^{1/2} + 4.8)$ eV, $E_{LUMO} = E_{HOMO} + E_g^{OPT}$ eV, where $E_{OX}^{1/2}$ was derived from the anodic or cathodic peak potential of a quasi-reversible oxidation wave of the complex, and E_g^{OPT} is the energy band gap estimated from the low-energy edge of the absorption spectra from the samples. The HOMO and LUMO energy levels for the other used materials were obtained from the literatures.[16]

Fabrication and testing of the NIR-PLEDs-IA/1B

Each of the **NIR-PLEDs-IA/1B** was fabricated on ITO (Indium tin oxide) coated glass

substrates with a sheet resistance of 20 Ω per square. Patterned ITO coated glass substrates were washed with acetone, detergent, D. I. water and isopropanol in an ultrasonic bath. After being exposed under oxygen plasma for 20 min, PEDOT:PSS from water solution was spin-coated (at 4800 rpm) on the substrate followed by drying in a vacuum oven at 130 °C for 30 min, giving a film of 50 nm in thickness. The DCM solution (10 mg/mL) of the mixture of PVK, OXD7 and one of the C_1-symmetric [Ir(C^N^1)(C^N^2)(N^O)]-*tris*-heteroleptic Ir(III)-complexes **1-2** as the emitting layer was prepared under an N_2 atmosphere and spin-coated (at 2100 rpm) on the PEDOT:PSS layer with a thickness of 50 nm. The TmPyPB layer (45 nm) was thermally deposited onto the emitting layer. Finally, a thin layer (1 nm) of LiF followed by Al capping layer (100 nm) was deposited onto the substrate under vacuum (5 × 10^{-6} Pa). Current density-voltage (*J-V*) characteristics were collected using a Keithley 2400 source meter equipped with a calibrated silicon photodiode. The NIR EL irradiance (*R*) was measured through a PR735 Spectra Scan spectrometer. The external quantum efficiency (η_{EQE}) of the NIR emission was obtained by measuring the irradiance in the forward direction and assuming the external emission profile to Lambertian.

Testing of molecular orientation of the emitting layer doped with the geometrical isomer 1a or 1b

As to the experimental determination of molecular orientation of their doped EMLs, it was investigated by variable-angle spectroscopic ellipsometry (VASE) method. The DCM solution (10 mg/mL) of the mixture of PVK (poly-(*N*-vinylcarbazole), OXD7 (1,3-*bis*(5-(4-*tert*-butyl-phenyl)-1,3,4-oxadiazol-2-yl)benzene) and one of the geometrical isomers **1a** and **1b** with a

stipulated wt% ratio of 65:30:5 as the EML-**1a**/EML-**1b** was prepared under a N_2 atmosphere and spin-coated (at 2100 rpm) on the Si wafer substrate with a thickness of 50 nm. The EMLs also with the 50 nm thickness like their **NIR-PLEDs-1A-1B** were spin-coated onto a Si wafer substrate treated with a piranha solution for the VASE (EC-400 (M2000U), J. A. Woollam *Co*.) measurement.

References

1   J. H. Palmer, A. C. Durrell, Z. Gross, J. R. Winkler and H. B. Gray, *J. Am. Chem. Soc.*, 2010, **132**, 9230-9231.

2   G. N. Li, Y. Zou, Y. D. Yang, J. Liang, F. Cui, T. Zheng, H. Xie and Z. G. Niu, *J. Fluoresc.*, 2014, **24**, 1545-1552.

3   S. Kesarkar, W. Mróz, M. Penconi, M. Pasini, S. Destri, M. Cazzaniga, D. Ceresoli, P. R. Mussini, C. Baldoli, U. Giovanella and A. Bossi, *Angew. Chem. Int. Ed.,* 2016, **55**, 2714-2718.

4   (a) H. B. Sun, L. J. Yang, H. R. Yang, S. J. Liu, W. J. Xu, X. M. Liu, Z. Z. Tu, H. Q. Su, Q. Zhao and W. Huang, *RSC Adv.*, 2013, **3**, 8766-8776; (b) S. Yi, J.-H. Kim, Y.-J. Cho, J. Lee, T.-S. Choi, D. W. Cho, C. Pac, W.-S. Han, H.-J. Son and S. O. Kang, *Inorg. Chem.*, 2016, **55**, 3324-3331.

5   G. R. Fu, H. Zheng, Y. N. He, W. T. Li, X. Q. Lü and H. S. He, *J. Mater. Chem. C,* 2018, **6**, 10589-10596.

6   G. M. Sheldrick, *SHELXL-97, Program for Crystal Structure Refinement*, University of Göttingen, Göttingen, Germany, 1997.

7   G. M. Sheldrick, G. M. *SADABS*, University of Göttingen, Göttingen, Germany, 1996.

8   (a) C. Jamorski, M. E. Casida, D. R. Salahub, *J. Chem. Phys.,* 1996, **104**, 5134-5147; (b) M. Petersilka, U. J. Grossmann and E. K. U. Gross, *Phys. Rev. Lett.,* 1996, **76**,1212-1215; (c) R. Bauernschmitt, R. Ahlrichs, F. H. Hennrich and M. M. Kappes, *J. Am. Chem. Soc.,* 1998, **120**, 5052-5059; (d) M. E. Casida, *J. Chem. Phys.*, 1998, **108**, 4439-4449; (e) R. E. Stratmann, G. E. Scuseria and M. J. Frisch, *J. Chem. Phys.*, 1998, **109**, 8218-8224.

9   W. R. Wadt and P. J. Hay, *J. Chem. Phys.,* 1985, **82**, 284-298.

10   P. J. Hay and W. R. Wadt, *J. Chem. Phys.,* 1985, **82**, 299-310.

11   T. Lu, Multiwfn Manual, version 3.6 (dev), Section 3.21.1 and 3.21.8, available at http://sobereva.com/multiwfn.

12   P. Ros and G. C. A. Schuit, *Theor. Chim. Acta,* 1966, **4**, 44-63.

13   T. Lu and F. W. Chen, *J. Comput. Chem.,* 2012, **33**, 580-592.

14   M. J. Frisch, G. W. Trucks, H. B. Schlegel, G. E. Scuseria, M. A. Robb, J. R. Cheeseman, G. Scalmani, V. Barone, B. Mennucci, G. A. Petersson, H. Nakatsuji, M. Caricato, X. Li, H. P. Hratchian, A. F. Izmaylov, J. Bloino, G. Zheng, J. L. Sonnenberg, M. Hada, M. Ehara, K. Toyota, R. Fukuda, J. Hasegawa, M. Ishida, T. Nakajima, Y. Honda, O. Kitao, H. Nakai, T. Vreven, J. A. Montgomery, Jr., J. E. Peralta, F. Ogliaro, M. Bearpark, J. J. Heyd, E. Brothers, K. N. Kudin, V. N. Staroverov, R. Kobayashi, J. Normand, K. Raghavachari, A. Rendell, J. C. Burant, S. S. Iyengar, J. Tomasi, M. Cossi, N. Rega, J. M. Millam, M. Klene, J. E. Knox, J. B. Cross, V. Bakken, C. Adamo, J. Jaramillo, R. Gomperts, R. E. Stratmann, O. Yazyev, A. J. Austin, R. Cammi, C. Pomelli, J. W. Ochterski, R. L. Martin, K. Morokuma, V. G. Zakrzewski, G. A. Voth, P. Salvador, J. J. Dannenberg, S. Dapprich, A. D. Daniels, ö.

Farkas, J. B. Foresman, J. V. Ortiz, J. Cioslowski, D. J. Fox, Gaussian 09, Revision D.01, Gaussian, Inc., Wallingford CT, 2009.

15   H. Y. Chen, C. T. Chen and C. T. Chen, *Macromolecules,* 2010, **43**, 3613-3623.

16   E. Zysman-Colman, S. S. Ghosh, G. Xie, S. Varghese, M. Chowdhury, N. Sharma, D. B. Cordes, A. M. Z. Slawin and I. D. W. Samuel, *ACS Appl. Mater. & Interfaces,* 2016, **8**, 9247-9253.

Table S1 Crystal data and structure refinement for the geometrical isomers **1a**·CHCl$_3$ and **1b**

Complex	1a·CHCl$_3$	1b
Empirical formula	C$_{35}$H$_{23}$Cl$_3$IrN$_3$O$_3$S	C$_{34}$H$_{22}$IrN$_3$O$_3$S
Formula weight	864.13	744.81
Crystal system	triclinic	monoclinic
Space group	*P-1*	*P2(1)/c*
a/Å	10.3518(17)	12.8035(6)
b/Å	11.8897(19)	8.8572(4)
c/Å	13.966(2)	23.9095(12)
α/°	87.779(2)	90
β/°	85.629(3)	100.6980(10)
γ/°	68.686(3)	90
V/Å^3	1596.6(4)	2664.3(2)
Z	2	4
ρ/g·cm^{-3}	1.798	1.857
Crystal size/mm	0.25×0.22×0.20	0.27×0.23×0.19
μ(Mo-Kα)/mm^{-1}	4.540	5.134
Data/restraints/parameters	6365/6/416	6058/0/380
Quality-of-fit indicator	1.010	1.153
No. unique reflections	6365	5068
No. observed reflections	8861	32320
Final *R* indices [*I* > 2σ(*I*)]	0.0663	0.1454
	0.1728	0.3053
R indices (all data)	0.0957	0.1463
	0.2058	0.3081

Table S2 The relevant bond lengths (Å) and bond angles (°) for the geometrical isomers

1a·CHCl$_3$ and **1b**

Complex	**1a**·CHCl$_3$	**1b**
Ir(1)-C(1)	2.008(11)	1.994(11)
Ir(1)-C(18)	1.964(15)	2.011(6)
Ir(1)-N(1)	2.039(10)	2.041(6)
Ir(1)-N(2)	2.025(11)	2.044(7)
Ir(1)-N(3)	2.149(10)	2.128(6)
Ir(1)-O(1)	2.201(9)	2.200(6)
C(1)-Ir(1)-C(18)	89.9(5)	92.1(3)
C(1)-Ir(1)-N(1)	80.8(4)	79.0(3)
C(1)-Ir(1)-N(2)	99.8(4)	103.6(3)
C(1)-Ir(1)-N(3)	172.2(5)	95.0(2)
C(1)-Ir(1)-O(1)	95.5(4)	170.3(3)

Table S3 The photo-physical properties of the C_1-symmetric [Ir(C^N^1)(C^N^2)(N^O)]-*tris*-heteroleptic Ir(III)-complex isomers [Ir(iqbt)(ppy)(hpa)]-**1a/1b** versus the [Ir(C^N)$_2$(N^O)]-*bis*-heteroleptic by-products [Ir(iqbt)$_2$(hpa)] and [Ir(ppy)$_2$(hpa)] in degassed CH$_2$Cl$_2$ solution at room temperature or 77 K

Comp.	Absorption[a]	Emission[a] (RT)						Emission[a] (77 K)	
	λ_{abs} [nm]	λ_{em} [nm]	S_M^c	τ [μs]	Φ_{PL}	k_r^b (10^5 s^{-1})	k_{nr}^b (10^6 s^{-1})	λ_{em} [nm]	$S_M^{[c]}$
1a	226, 263, 454, 515	697, 756 (sh)	0.32	0.33	0.27	8.2	2.2	697, 763 (sh)	0.29
1b	227, 262, 453, 514	696, 760 (sh)	0.34	0.38	0.33	8.7	1.8	691, 755 (sh)	0.28
[Ir(ppy)$_2$(hpa)]	234, 262, 396, 430, 476	506, 522(sh)	0.93	0.22	0.20	9.1	3.6	-	-
[Ir(iqbt)$_2$(hpa)]	314, 420, 448, 492, 672	700, 760(sh)	0.88	2.13	0.13	0.61	0.41	-	-

[a]Measured in degassed CH$_2$Cl$_2$ solution;

[b]$k_r = \Phi_{PL}/\tau$, $k_{nr} = (1 - \Phi_{PL})/\tau$;

[c]Huang–Rhys factor (S_M) is calculated from the peak heights and energies of (0−0) and (0−1) band, $S_M = (I_{0-1}/I_{0-0})$ ($\bar{v}_{0-0}/\bar{v}_{0-1}$).

Table S4 Frontier orbital energy and electron density distribution for the geometrical

isomers **1a** and **1b** on the basis of their optimized S_0 geometries

complex	MO	Contribution of metal d_π orbitals and π orbitals of ligand to MOs (%)			
		Ir	iqbt	ppy	hpa
1a	LUMO+1	1.99	4.24	9.16	84.61
	LUMO	4.54	89.39	0.35	5.72
	HOMO	24.29	63.28	9.68	2.76
	HOMO-1	38.46	32.14	8.59	20.81
1b	LUMO+1	2.19	0.81	2.65	94.35
	LUMO	5.16	92.51	0.40	1.94
	HOMO	29.40	51.74	15.20	3.66
	HOMO-1	7.79	41.60	43.03	7.59

Table S5 The calculated orbital transition analyses for the geometrical isomers **1a** and **1b** by

TD-DFT calculations with the IFCT analyses at the B3LYP level

Comp.	state	λ (nm)	E (eV)	oscillator (f)	transition (contrib.)	assignment			
1a	$S_0 \rightarrow S_1$	508	2.4416	0.1038	HOMO $\rightarrow$ LUMO (94.0%)	^{1}ILCT 43.74%		^{1}MC	1.40%
						^{1}MLCT 29.32%		^{1}LMCT	3.15%
						^{1}LLCT 22.39%			
	$S_0 \rightarrow T_1$	692	1.7916	0.0000	HOMO $\rightarrow$ LUMO (86.6%)	^{3}ILCT 72.66%		^{3}MC	0.82%
						^{3}MLCT 15.93%		^{3}LMCT	4.09%
						^{3}LLCT 6.49%			
	$T_1 \rightarrow S_0$	899	1.3797	0.0000	HOMO $\rightarrow$ LUMO (94.1%)	^{3}ILCT 78.73%		^{3}MC	0.76%
						^{3}MLCT 16.68%		^{3}LLCT	3.83%
1b	$S_0 \rightarrow S_1$	523	2.3709	0.6888	HOMO $\rightarrow$ LUMO (94.9%)	^{1}ILCT 48.00%		^{1}MC	1.52
						^{1}MLCT 27.88%		^{1}LMCT	3.64
						^{1}LLCT 18.97%			
	$S_0 \rightarrow T_1$	699	1.7745	0.0000	HOMO $\rightarrow$ LUMO (86.4%), HOMO-1 $\rightarrow$ LUMO (8.0%)	^{3}ILCT 67.60%		^{3}MC	1.04%
						^{3}MLCT 19.73%		^{3}LLCT	8.07%
	$T_1 \rightarrow S_0$	918	1.3510	0.0000	HOMO $\rightarrow$ LUMO (92.9%), HOMO-1 $\rightarrow$ LUMO (5.6%)	^{3}ILCT 74.21%		^{3}MC	1.04%
						^{3}MLCT 13.75%		^{3}LMCT	5.98%
						^{3}LLCT 5.03%			

Table S6 The transition dipole moments $\Delta\mu$ comparison for the geometrical isomers **1a** and

1b upon DFT calculations based on their corresponding optimized T_1 and S_0 states

Complex	State	x	y	z	$\left|\vec{\mu}\right|$ (D)	θ (°)	$\left|\Delta\vec{\mu}\right|$ (^{1}T-^{0}S) (D)
1a	S_0	4.5504	-2.4933	5.5858	7.6239	11.85	1.92
	T_1	6.1918	-1.5039	5.7430	8.5780		
1b	S_0	1.4259	-0.6567	-6.5646	6.7497	19.21	2.23
	T_1	-0.7687	-1.0001	-6.4108	6.5337		

Table S7 NIR performances of the **NIR-PLEDs-1A/1B** based on the C_1-symmetric [Ir(C^N^1)(C^N^2)(N^O)]-*tris*-heteroleptic Ir(III)-complexes [Ir(iqbt)(ppy)(hpa)] (**1a** and **1b**)

Device	λ_{em} (nm)	V_{on} (V)	η_{EQE}^{Max} (%)	R^{Max} (mW/sr·m^2)	Efficiency-roll-off (%)
NIR-PLED-1A	694, 758(sh)	6.1	5.4	1952.9	3.6
NIR-PLED-1B	700, 760(sh)	5.6	3.3	1499.0	2.1

Table S8 Summarized results of coefficients (maximum ordinary coefficient k_o^{max}, maximum extraordinary coefficient k_e^{max}), order parameters (S), and horizontal dipole ratios ($h/(h+v)$) of the spin-coated EMLs-**1a/1b** for the **NIR-PELDs-1A/1B** composed of PVK-OXD7 (65:30, wt%) as the *co*-host and each of the Ir(III)-complexes **1a-1b** as the dopant at 5 wt% doping level

EML	k_e^{max} (λ)	k_o^{max} (λ)	S^a	$h/(h+v)^b$
PVK:OXD7:**1a** (65:30:5; wt%)	0.636 (233 nm)	0.854 (235 nm)	-0.09	0.72
PVK:OXD7:**1b** (65:30:5; wt%)	0.481 (236 nm)	0.766 (240 nm)	-0.14	0.76

$$_a\ S = \frac{k_e^{max} - k_o^{max}}{k_e^{max} + 2k_o^{max}}$$

$$_b\frac{h}{h + v} = \frac{2(1 - S)}{3}$$

Scheme S1 Synthetic scheme of the [Ir(C^N)(C'^N')(N''^O)]-*tris*-heteroleptic geometrical isomers (**1a** and **1b**) and the [Ir(C^N)$_2$(N^O)-*bis*-heteroleptic by-products.
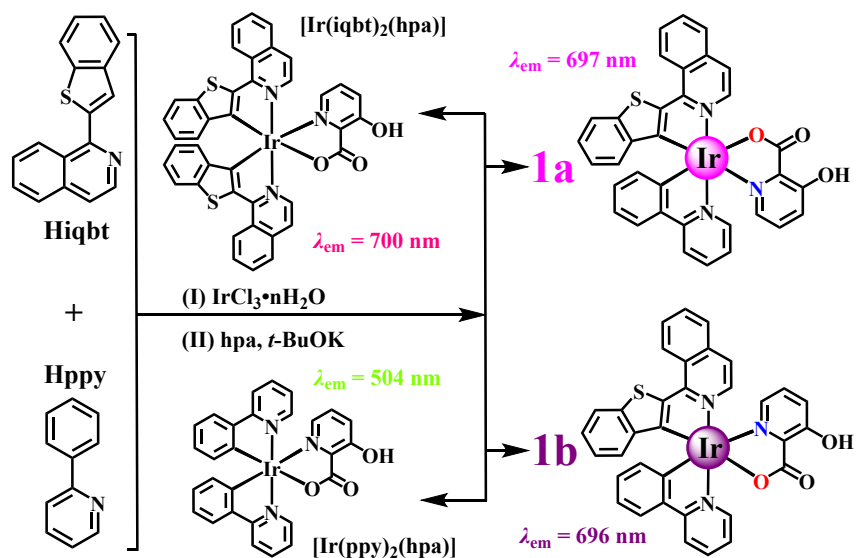
Figure S1 The ^{1}H NMR spectra of the [Ir(C^N)(C'^N')(N''^O)]-*tris*-heteroleptic geometrical isomers (**1a** and **1b**) in CDCl$_3$ at room temperature
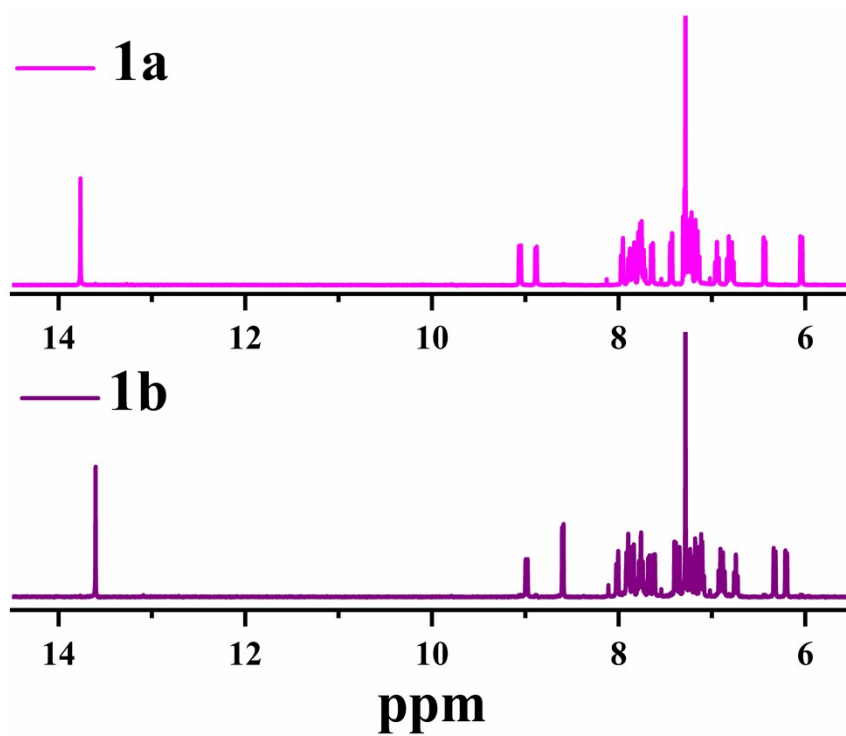
Figure S2 The TG (thermogravimetric analysis) curves for the [Ir(C^N)(C'^N')(N''^O)]-*tris*-

heteroleptic geometrical isomers (**1a** and **1b**).
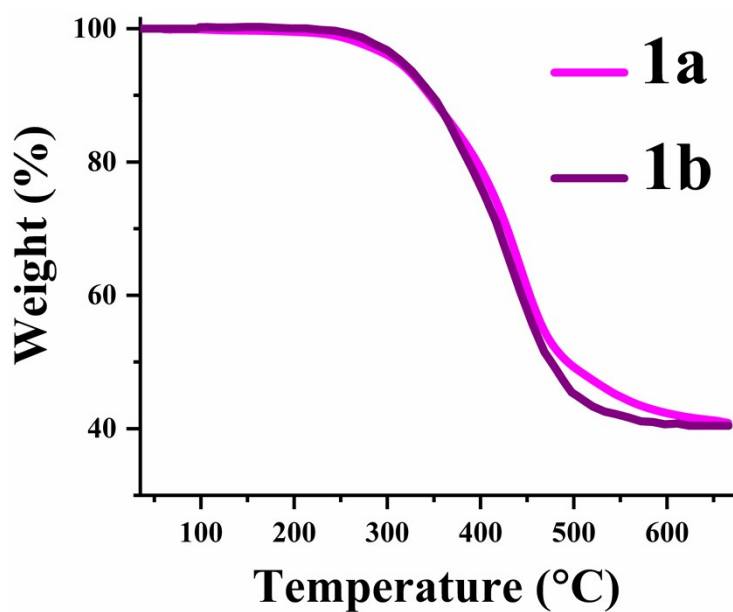
Figure S3 The normalized UV-visible absorption spectra of the HC^N[1] main ligand **Hiqbt**, the

HC^N[2] ligands **Hppy** and the **hpa**-ancillary ligand in degassed CH_2Cl_2 solutions at room
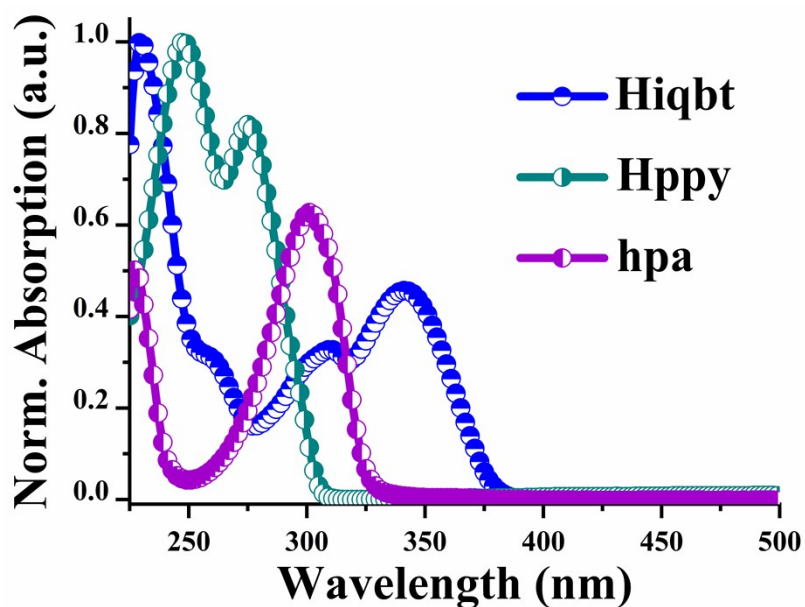
temperature.

Figure S4 The normalized UV-visible absorption of the two by-products ([Ir(iqbt)$_2$(hpa)] and [Ir(ppy)$_2$(hpa)]) in degassed CH$_2$Cl$_2$ solutions at room temperature.
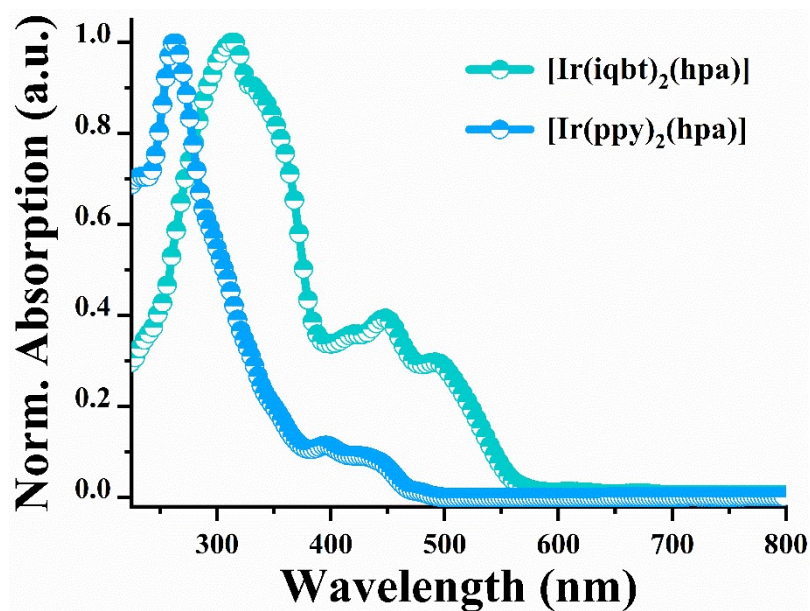
Figure S5 The normalized emission spectra of the two by-products ([Ir(iqbt)$_2$(hpa)] and [Ir(ppy)$_2$(hpa)]) in degassed CH$_2$Cl$_2$ solutions at room temperature.
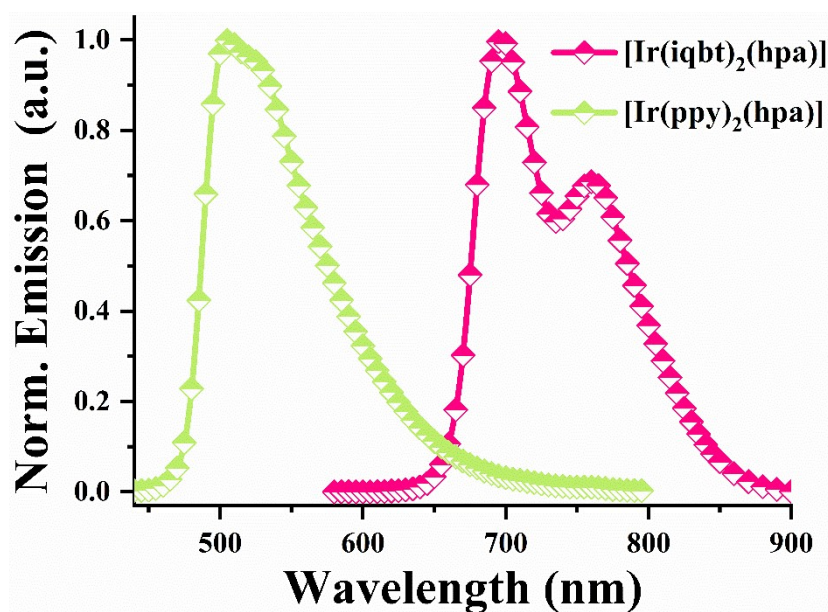
Figure S6 The normalized emission spectra of the HC^N^1 main ligand **Hiqbt**, the HC^N^2 ligands **Hppy** and the **hpa**-ancillary ligand in degassed CH_2Cl_2 solutions at room temperature.
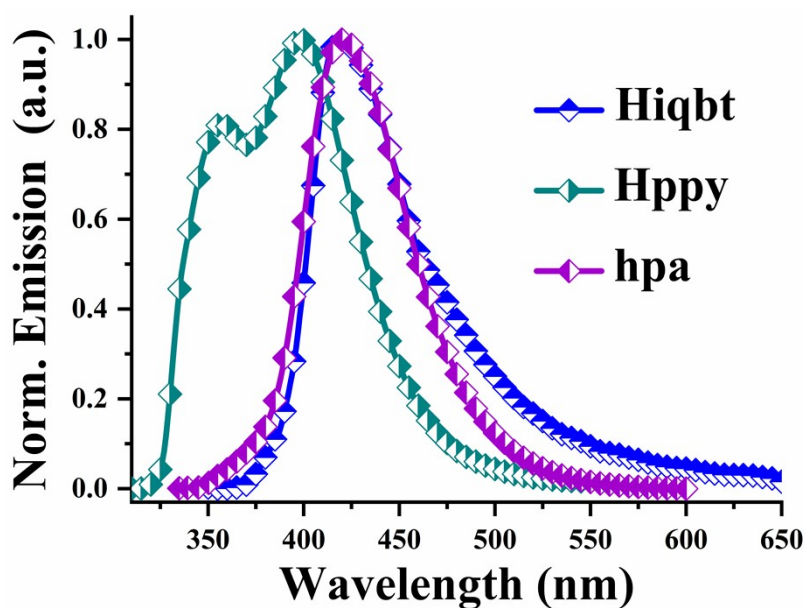
Figure S7 The normalized emission spectra for the C_1-symmetric [Ir(C^N^1)(C^N^2)(N^O)-*tris*-heterolepticIr(III)-complexes [Ir(iqbt)(ppy)(hpa)] (**1a** and **1b**, λ_{ex} = 370 nm) in degassed CH_2Cl_2 solution at 77 K.
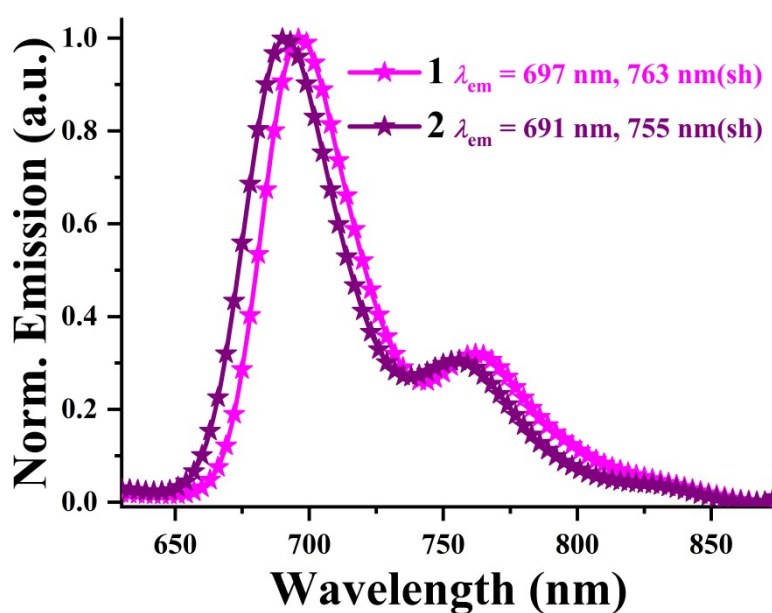
Figure S8 The HOMO and LUMO patterns for the [Ir(C^N)(C'^N')(N''^O)]-*tris*-heteroleptic

geometrical isomers (**1a** and **1b**) based on their corresponding optimized S_0 geometries.
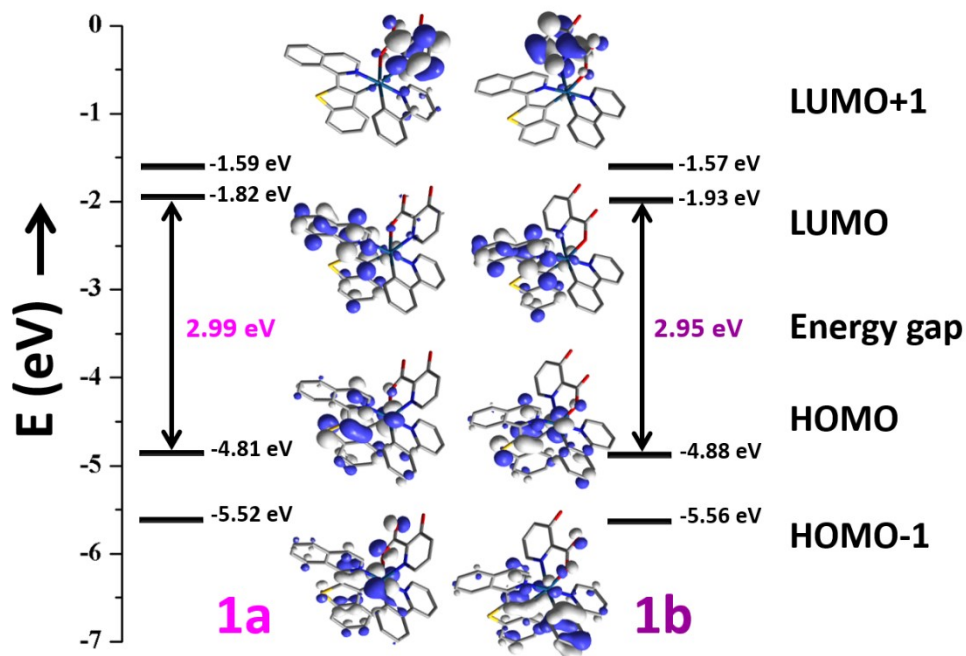
Figure S9 The HOMO and LUMO patterns for the [Ir(C^N)(C'^N')(N''^O)]-*tris*-heteroleptic

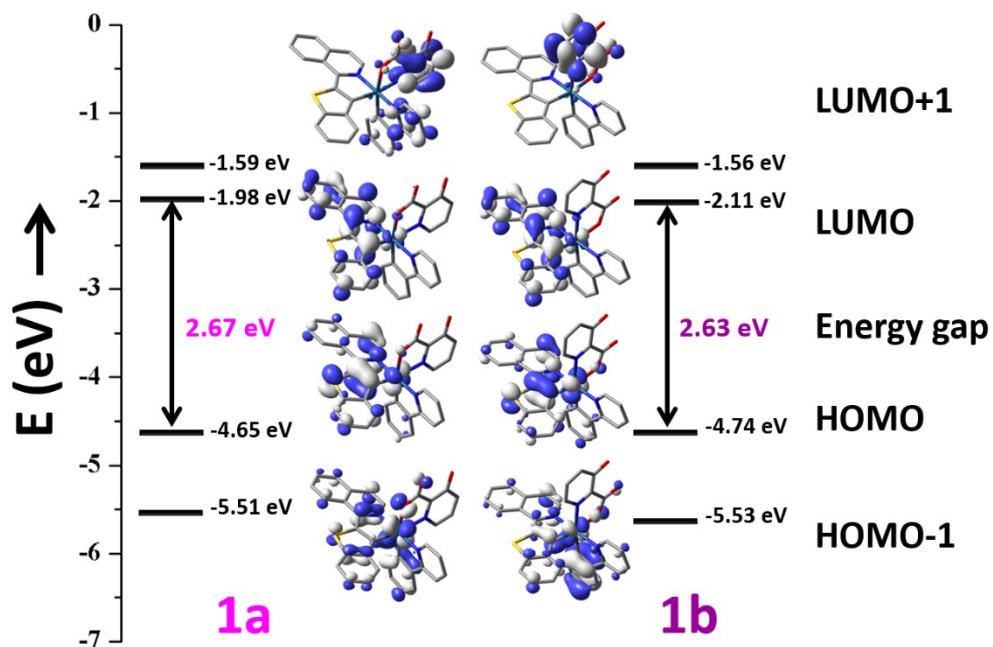geometrical isomers (**1a** and **1b**) based on their corresponding optimized T_1 geometries.

Figure S10 The CV (cyclic voltammogram) curves of the [Ir(C^N)(C'^N')(N''^O)]-*tris*-heteroleptic geometrical isomers (**1a** and **1b**) recorded *versus* Fc⁺/Fc in degassed MeCN solution at room temperature under a N_2 atmosphere (scan rate = 100 mV/s).
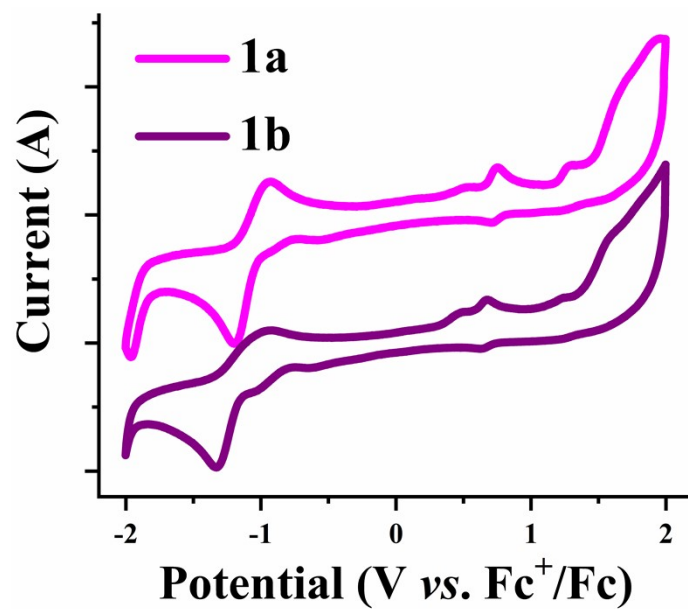

Figure 11 The voltage-relative electroluminescent spectra of **NIR-PLEDs-1A/1B** based on the
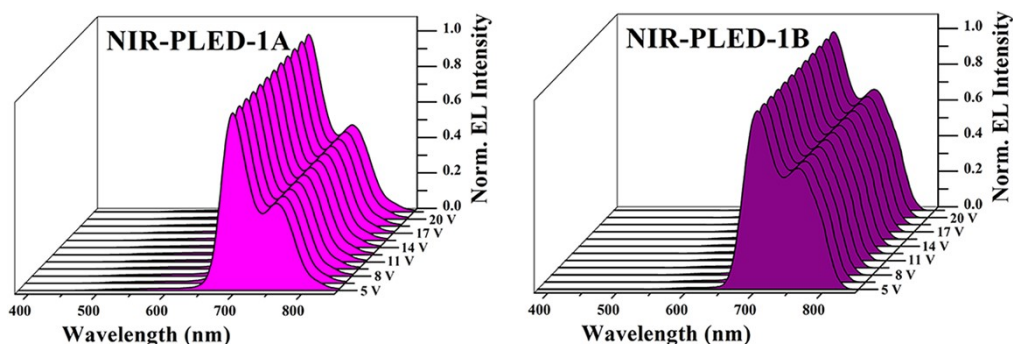
two Ir³⁺-complexes [Ir(iqbt)(ppy)(hpa)]-**1a/1b**.

Figure S12 Refractive index (*n*; a-b) and coefficient (*k*; c-d) in ordinary (n_o/k_o) and extraordinary (n_e/k_e) modes of the EML-**1a** and EML-**1b** doped with the corresponding geometrical isomer **1a** and **1b**.